Supplementary Materials for

Spatial Colocalization and Functional Link of Purinosomes with Mitochondria

Jarrod B. French[1†*], Sara A. Jones[2†‡], Huayun Deng[3], Anthony M. Pedley[4], Doory Kim[2,6], Chung Yu Chan[5], Haibei Hu[3§], Raymond J. Pugh[4], Hong Zhao[4], Youxin Zhang[2], Tony Jun Huang[5], Ye Fang[3*], Xiaowei Zhuang[2,6,7*], Stephen J. Benkovic[4*]

correspondence to: jarrod.french@stonybrook.edu, fangy2@corning.com, zhuang@chemistry.harvard.edu, sjb1@psu.edu

This PDF file includes:

Other Supplementary Materials for this manuscript includes the following:

Materials and Methods

Chemicals for drug treatment studies

Unless otherwise stated, all chemicals used in drug treatment studies were purchased from Sigma-Aldrich, dissolved in cell culture grade dimethyl sulfoxide (DMSO), and used at the following concentrations: MKT-077 at 10 μM; 17-AAG at 100 nM; 4,5,6,7-tetrabromo-2-azabenzimidazole (TBB) at 25 μM; 2-dimethylamino-4,5,6,7-tetrabromobenzimidazole (DMAT) at 25 μM; antimycin A at 10 μM; oligomycin at 10 μM; rotenone at 100 nM; 2-deoxyglucose (2-DG) at 1 mM; rapamycin (Selleckchem) at 100 nM. All compounds were used without further purification.

Constructs used for imaging studies

Conventional fluorescence microscopy of purinosomes was conducted as previously reported using FGAMS-GFP as a marker for purinosomes *(5, 11, 12, 16)*. For STORM imaging, FGAMS-mEos2 and FGAMS-mMaple3 were constructed from FGAMS-GFP using standard molecular biology techniques.

Cell culture

HeLa cells (ATCC) were maintained in either 'purine rich' conditions (MEM with Earle's salts and L-glutamine supplemented with 10% (v/v) FBS, Atlanta Biologicals) or 'purine-depleted' conditions [RPMI 1640 with L-glutamine supplemented with 5% (v/v) dialyzed (25 kDa MWCO) FBS]. The cells were transfected in OPTI-MEM using Lipofectamine 2000 (Life Technologies) following manufacturer's protocol. The cells were imaged or fixed 20-30 hours post transfection.

Live cell fluorescence microscopy

Live HeLa cell samples were washed three times for 5 min incubations with buffered saline solution [BSS: 20 mM HEPES (pH 7.4), 135 mM NaCl, 5 mM KCl, 1 mM $MgCl_2$, 1.8 mM $CaCl_2$, and 5.6 mM glucose] before imaging. Cells were imaged at ambient temperature (25 °C) using a Nikon TE-2000E inverted microscope equipped with a 60x1.49 numerical aperture objective and a photometrics CoolSnap ES2 CCD detector. GFP fluorescence was visualized using an S484/15x excitation filter, S517/30m emission filter, and Q505LP/HQ510LP dichroic (Chroma Technology). The OFP signal was obtained by using an S555/25x excitation filter, 605/40m emission filter, and Q575LP/HQ585LP dichroic (Chroma Technology). Nikon NIS-Elements (v. 3.0) was used for collecting images samples, which were viewed using a mercury fiber illuminator. To view mitochondria in live-cell conventional imaging experiments (Figure S1), MitoTracker Red (Life Technologies) was used according to the manufacturer's protocol.

Purinosome content was calculated by dividing the number of transfected cells containing purinosomes (FGAMS-GFP puncta) by the total number of transfected cells. Purinosome content was reported as a percentage (equal to the fraction of cells harboring purinosomes × 100). For drug treatments, the cells were treated for 1 hour with the listed concentrations of the small molecules or with DMSO (untreated vehicle control) and maintained at 37 ºC and 5% CO_2 prior to analysis as outlined above. Three independent samples were analyzed; each sample had at least 100 cells counted.

Cell fixation and immunostaining

Cells were grown as detailed above and washed 3 times with phosphate buffered saline (PBS) prior to fixing with freshly made 3% (v/v) paraformaldehyde (Electron Microscopy Sciences) and 0.1% (v/v) glutaraldehyde (Electron Microscopy Sciences) in PBS for 15-20 min at room temperature. Cells were rinsed twice with PBS and reduced with a solution of 1 mg/mL sodium borohydride for 5 minutes or 50 mM glycine for 30 minutes and rinsed three times with PBS. After rinsing, the samples were blocked with 3% (w/v) bovine serum albumin (IgG-free, Jackson ImmunoResearch) and 0.2% (v/v) Triton X-100 in PBS for 60 min. Primary and secondary antibodies were diluted in the same blocking buffer and incubated for 60 min at room temperature. Between antibody incubations, cells were washed three times with a wash solution (0.2% (w/v) BSA and 0.05% (v/v) Triton X-100 in PBS), 5 min per wash. After incubation, cells were again washed and then post-fixed in 3% (v/v) paraformaldehyde and 0.1% (v/v) glutaraldehyde for 10 min. Samples were rinsed three times in PBS and stored at 4 ºC or imaged immediately. Antibodies used include: anti-Tom20 (Santa Cruz Biotechnologies, sc-11415 or sc-17764), anti-GFP (Life Technologies, A11122 or 1241447), and anti-Myc (Abcam, ab9132).

STORM imaging and analysis

Samples were imaged using STORM in PBS with the addition of a thiol-based switching agent [either 100 mM mercaptoethylamine (MEA) at pH 8.5 or 136 mM β–mercaptoethanol), 5% (w/v) glucose and oxygen scavenging enzymes (0.5 mg/mL glucose oxidase (Sigma-Aldrich), and 40 μg/mL catalase (Roche Applied Science)]. All two-color 3D STORM experiments were performed on an Olympus IX71 inverted optical microscope as previously described *(22, 23)*. Briefly, six laser beams at wavelengths of 657 nm (RCL-300-656; Crystalaser), 561 nm (Sapphire 561-250; Coherent), 532 nm (GCL-200-L; Crystalaser), 514 nm (Sapphire 514-50; Coherent), 460 nm (Sapphire 460-10; Coherent) and 405 nm (CUBE 405-50C; Coherent) were individually controlled by mechanical shutters (Uniblitz LS6T2; Vincent Associates) and an acousto-optic tunable filter (AOTF PCAOM NI VIS; Crystal Technology). All laser lines were combined and coupled into an optical fiber (Oz Optics), and the fiber output was collimated and focused into a high numerical aperture oil immersion objective (100x UPlanSApo, NA1.4; Olympus). Output fluorescence was imaged onto a back-illuminated EMCCD camera (iXON DU-897; Andor). To stabilize the focus during data acquisition, an 830 nm fiber-coupled diode laser (LPS-830-FC; Thorlabs) was introduced into the microscope in a separate objective-type TIRF path. The reflected IR beam from the coverglass-water interface was directed to a quadrant photodiode. The position readout of the quadrant photodiode provided feedback to a piezo objective positioner (Nano-F100; MadCity Labs), keeping the focal drift to less than 20 nm *(23)*.

For two-color imaging of Alexa 647 and mEos2 (or mMaple3), two imaging beams (561 nm and 657 nm) and an activation beam (405 nm) were reflected by a custom-designed polychroic mirror (zt405/488/561/640rpc; Chroma) into the objective. Fluorescence emissions from Alexa 647 and mEos2 (or mMaple3) were separated by a 630 nm longpass dichroic mounted on a commercial beamsplitting device (Dual-View; Photometrics). The short-wavelength channel was filtered with a bandpass filter (FF01-607/70; Semrock) for mEos2 (or mMaple3). The long-wavelength channel was filtered

with a bandpass filter (ET705/72m; Chroma) for Alexa 647. In addition to the bandpass filters, a double notch filter (NF01-568/647; Semrock) was added before the Dual-View to block the two excitation beams. For 3D localization, a cylindrical lens with a focal length of 100 cm was inserted into the imaging optical path.

STORM images were generated using similar methods as previously described *(23)*. Briefly, images of individual molecules were identified and fit to an elliptical Gaussian function to obtain the centroid position coordinates (x_0 and y_0) and the Gaussian widths (d_x and d_y). The lateral position of the molecule were determined as x_0 and y_0, while the z position was calculated from d_x and d_y using a calibration curve independently determined by imaging 100-nm fluorescent bead (Tetraspeck; Invitrogen) on a coverglass while scanning in z. The z position was then corrected for refractive index mismatch between glass and the imaging medium as previously described *(22)*. Sample drift during the image acquisition in both lateral and axial directions was measured and corrected via correlation analysis between images taken in different time windows as described previously *(23)*. For two-color imaging of Alexa 647 and mEos2 (or mMaple3), the two STORM images were aligned by a third-order polynomial warping map in 3D obtained from bead calibration images.

Purinosomes and mitochondria content and colocalization were determined using custom written Matlab code. High-resolution images of 2D projections of 3D STORM images of both mitochondria and purinosomes were subjected to median filtering and intensity thresholding (according to Otsu's thresholding algorithm). Object boundaries were then determined using 8-point connectivity with a size threshold of 100 nm. Mitochondria boundaries were dilated by 1 pixel to account for erosion during boundary identification. The Euclidean distance between mitochondria-containing pixels and purinosome-containing pixels was then used to determine the overlap matrix. Mitochondria-purinosome boundary-to-boundary distances of less than 100 nm for greater than 10% of pixels in the purinosome were classified as positive colocalization. This threshold takes into account not only the finite image resolution but also allows for some spatial separation between identified objects since the labeled marker proteins (core purinosome component FGAMS and mitochondrial protein TOM20) are not thought to be direct interaction partners.

To determine whether the fraction of purinosomes colocalized with mitochondria was larger than the fraction expected for a random distribution, we used two different methods to randomize the purinosome distribution. First, existing STORM data was used to simulate a random distribution of purinosomes within the cell. Purinosomes show no obvious bias towards cytoplasmic location (i.e. perinuclear or otherwise), so purinosome position within the entire cell boundary was randomized with the mitochondria distribution left unchanged. To randomize the purinosome distribution, the centroid position of each identified purinosome was randomly assigned to a pixel location within the user-defined cell boundary (nuclear pixels were excluded) while leaving all other purinosome shape and size parameters unchanged. Colocalization between the randomized purinosomes and the imaged mitochondria was then calculated as described above. For each true STORM image, 10 randomized purinosome distributions were simulated and averaged for comparison. $N = 26$ STORM images were compared with randomized images and statistical significance of the difference in colocalization

observed in true STORM images and randomized images was determined using a paired t-test.

An alternative randomization method was to rotate the imaged purinosome distribution 90^o with respect to the imaged mitochondria distribution. If the distribution is random, the colocalization percentage with mitochondria should be independent of rotation. To avoid rotating purinosomes out of the cell boundaries, we identified the largest contiguous square region within the cell boundary for each STORM image and then rotated the purinosome image 90^o while leaving the mitochondria image unchanged. Within these identified square regions, the colocalization percentage of the imaged distribution was compared with that of its rotated counterpart. Paired t-test on these distributions was used to determined statistical significance, again using N = 26 STORM images. By cropping the analyzed cell area to its largest contiguous square region, we bias the analysis toward the perinuclear regions of the cell where the mitochondria density is often observed to be higher and hence the observed difference in colocalization in true STORM images and randomized images were smaller than that observed using the first randomization method. However, both randomization methods clearly showed that the fraction of purinosomes colocalized with mitochondria in the STORM images was statistically significantly larger than that observed in the images where the purinosomes were randomized.

To calculate both the purinosome properties and mitochondria distributions in response to rapamycin treatment, objects were identified in the STORM images as described above. The number of purinosomes per imaging field of view was then counted. The enclosed area of each purinosome was then used to calculate its effective diameter. The mitochondria content in response to rapamycin treatment was calculated by taking the number of signal-positive pixels identified within the mitochondria channel divided by the total number of pixels within the user-defined cell boundary (excluding the nucleus). Similarly, the mitochondria distribution was calculated by determining the Euclidean distance from each mitochondria-containing pixel to the centroid of the user-defined nuclear boundary.

Malate and lactate metabolite assays

A total of 1×10^7 HeLa cells were treated with a specific drug or DMSO vehicle control for 1 h at 37 ºC and 5% CO_2, harvested, and washed once with PBS. For metabolite extraction, the cell pellet was suspended in 300 μL methanol followed by addition of 300 μL water. The resuspended pellet was flash frozen with liquid nitrogen and lysed by 5 min incubation on ice. After the first round of lysis, 400 μL chloroform was added followed by another round of lysis and centrifugation. A representative sample of the top layer (200 μL) was collected, dried down, and resuspended in 50 μL water for malate and lactate level determination using a Malate Colorimetric Assay Kit (Sigma-Aldrich, BioVision) or Lactate Colorimetric Assay Kit (Sigma-Aldrich) according to manufacturer's protocol. Samples were incubated for 60 min at 37 ºC in the dark, and absorbance readings at 450 nm were acquired using an EL311s microplate reader (Bio-Tek Instruments) at 30, 45, and 60 min to ensure the readings were stable. Data reported is from the 60 min time point.

Identification of proteins by mass spectrometry

Prior to extraction of mitochondria, 1×10^8 HeLa cells grown in medium depleted of purines were harvested, rinsed with PBS and treated with one of the four cross-linkers (dithiobis(succinimidyl proprionate), DSP; succinimidyl 3-(2-pyridyldithio)propionate, SPDP; succinimidyol (4-azidophenyl)1,3'-dithiopropionate, SADP; dimethyl 3,3'-dithiobispropionimidate-2HCl, DTBP; all from Pierce), following the manufacturer's protocol. Briefly, 1 mM final concentration of crosslinker was added to a solution of PBS or Hepes, pH 7.2 (for DSP), pH 7.5 (for SPDP), pH 8.0 (for DTBP) or pH 8.5 (for SADP) and the reaction was allowed to incubate for 2 hours on ice. The reaction was quenched with the addition of 50 mM Tris. For SADP, the sample was also irradiated with UV (265 nm) for 15 minutes. Mitochondria were isolated using a Mitochondria Isolation Kit for Mammalian Cells (Thermo Scientific) according to manufacturer's protocol. Mitochondria were further purified using a 4-step (15%- 40%) Percoll (Sigma-Aldrich) density gradient. Mitochondrial (-in-gel) and cytosolic (-in-solution) fractions were analyzed on a Thermo LTQ Orbitrap Velos mass spectrometer with a Dionex Ultimate 3000 nano-LC system was used to analyze tryptic peptides (extracted from gel). The resulting LC-MS2 data were processed by Proteome Discoverer 1.3 application (Thermo Scientific) and searched against a database containing the human protein sequences and the common contaminating protein sequences (downloaded from ftp://ftp.thegpm.org/fasta/cRAP, February 2014).

Western blot analyses

A total of 2×10^7 HeLa cells grown under purine-depleted (purinosome forming) conditions were transiently transfected with a plasmid encoding FGAMS-3×FLAG using Lipofectamine 2000 (Life Technologies) according to manufacturer's instructions and the FGAMS-3xFLAG levels were detected with anti-FLAG. FGAMS-3×FLAG mammalian expression vector was constructed using standard cloning techniques. At 24 h post-transfection, the cells were treated with 1 μM rapamycin (Selleckchem) prepared in DMSO for 1 h. A no drug (DMSO) control was performed to account for any differences due to DMSO. Cells were washed with PBS, harvested, and their mitochondria isolated using a Mitochondria Isolation Kit for Mammalian Cells (Thermo Scientific) according to manufacturer's instructions with exception of a second wash of the final mitochondria pellet with 500 μL reagent C. Soluble mitochondrial protein was extracted from the isolated and washed mitochondria pellet using 2% (w/v) CHAPS in TBS (vortex vigorously for 2 min followed by centrifugation of insoluble material at 12,000×g for 10 min). All steps were carried out on ice and in the presence of protease and phosphatase inhibitors. A total of 50 μg of lysate was loaded on each lane of a 10% denaturing polyacrylamide gel and transferred to PVDF membrane using a Trans-blot Turbo Transfer System (Bio-Rad). Blot was blocked with 5% (w/v) dry milk in TBST for 1 h prior to addition of primary antibody in 5% (w/v) dry milk in TBST. Primary antibodies were incubated with the blot overnight at a 1:1000 dilution. Incubation of the blot with HRP-conjugated goat-anti-rabbit secondary antibody (1:2000-4000) in 5% (w/v) dry milk in TBST proceeded for 1 h at room temperature and followed by addition of SuperSignal West Pico Chemiluminescent Substrate (Thermo Scientific) for 5 min prior to exposure on a Bio-Rad ChemiDoc XRS+ with ImageLab software. For pThr389-p70-S6K blocking and primary antibody probing, a 5% (w/v) BSA solution in TBST was used. Antibodies used for the Western blot analysis are as follows: FGAMS from Bethyl Laboratories

(A304-218A); ADSL from Bethyl Laboratories (A304-778A); VDAC1 from Cell Signaling Technology (4661), FLAG M2 from Sigma Aldrich (F1804), pThr389-p70-S6K from Cell Signaling Technology (9205) and p70-S6K from Cell Signaling Technology (9202).

DMR assays

Materials: Epic 384-well biosensor cell culture compatible microplates were obtained from Corning Incorporated. TBB and epinephrine (EPI) were obtained from Sigma-Aldrich. Everolimus was obtained from LC Laboratories. MISSION TRC shRNA kinome library was purchased from Sigma-Aldrich. shRNAs that generate siRNAs intracellularly are expressed from amphotropic lentivirus particles, allowing for quick, high throughput loss-of-function screens. The library contains 3109 different lentiviruses carrying shRNA sequences targeting 673 human kinase genes, each represented by a set of 3-5 individual clones targeting different regions of the gene sequence.

shRNA kinome screen: For shRNA transfection HeLa cells (ATCC) were seeded in the biosensor microplate at 25,000 cells per well suspended in 50µL of growth medium [DMEM, 10% (v/v) FBS, and 1% penicillin/streptomycin (all from Life Technologies)] and cultured at 37 ^{o}C under 5% CO_2 overnight. At day 2, the cells were washed twice using a plate washer (Bio-Tek Microplate Washers ELx405t and incubated with 10 µL of growth media with hexadimethrine bromide (10 mg/mL stock). The lentiviral particles as received were directly diluted to 5000 particles using 30µL growth media, and were then added to the cell biosensor plates at 28 µL/well. After a brief spin down at 800 rpm for 30 sec at room temperature and sitting in the cell culture hood for 10 min, the cell plates were cultured to allow for transfection. At day 3, the cell plates were washed twice and maintained in 40 µL of growth media. Afterwards, the cells were cultured for the next two days at 37˚C under 5% CO_2. At day 5, the transfection efficiency was first assessed based on GFP fluorescence of cells in a control plate infected with MISSION TurboGFP Control Transduction Particles, and DMR assays were then performed using an Epic® wavelength interrogation system (Corning Incorporated). This system consists of a temperature-control unit (28 ^{o}C), an optical detection unit and an on-board liquid handling unit with robotics. The detection unit is based on integrated fiber optics and enables kinetic measures of cellular responses with a time interval of ~15 sec. For DMR assays the cell plates were washed twice with assay buffer (Hank's Balanced Salt Solution containing 20mM HEPES) using the plate washer and maintained in 30 µL assay buffer. For shRNA screening, a sequential two-step DMR assay, each step lasting one hour, was employed, wherein the cells were first stimulated with 100nM EPI, and then stimulated with 20µM TBB. For inhibitor dose studies, HeLa cells were seeded at 25,000 cells per well in the biosensor plates and cultured overnight to achieve 95% confluency. After washed twice with assay buffer, the cells were pretreated with the kinase inhibitors for 1 h, and then sequentially stimulated with 100nM EPI and 20µM TBB. The EPI-induced and TBB-induced DMR were recorded separately. Solutions of small molecules were made by diluting the stored concentrated solutions with assay buffer and transferred into a 384-well polypropylene compound storage plate to prepare a compound source plate. Two compound source plates were made separately when two-step assays were performed. Both cell and compound source plates were incubated within the Epic system to reach thermal equilibrium (~1 h). After a 2 min baseline was recorded,

compounds were transferred using the on-board liquid handler. All DMR signals were buffer and solvent corrected.

Data analysis: Quantification of DMR was performed by analyzing the real responses at 50 min post-stimulation for both EPI- and TBB-induced DMR. The screening robustness was assessed based on the coefficient of variation (CV) and the difference between the positive controls (EPI and TBB with vehicle only) and the negative controls (Buffer and Buffer with vehicle only). The Z' factor was calculated using the formula of [1 – (3 x CV of the positive control + 3 x CV of the negative control) / (the mean of the positive control – the mean of the negative control)]. A Z' factor > 0.5 was considered robust. For the whole screens the Z' factors obtained for different controls were variable; that is, it is 0.4 to 0.5 for the TBB DMR, 0.3 for the EPI-potentiated TBB response, and 0.7 for the EPI -DMR. Therefore, we used an intra-plate approach to identify hits; that is, the alteration of the DMR of EPI, or the DMR of TBB after EPI pre-stimulation, was normalized to the plate median; that is for shRNA screens the EPI DMR in the shRNA transfected cells was normalized to that in the non-target lentivirus treated cells within the same plate, later of which was set to 100%. The TBB DMR after EPI pre-stimulation in the shRNA transfect cells was normalized to the TBB DMR after buffer pretreatment in the non-target lentivirus treated cells, later of which was set to 100%. A robust z-score (z-score in which the outlier-insensitive median and median absolute deviation (MAD) is substituted for the mean and standard deviation in the z-score calculation) was calculated for each shRNA treatment. The normalization strategy set the median robust z-score at 0, with a median absolute deviation of 1. shRNA screen hits were identified when at least two of the multiple clones for each kinase altered the DMR amplitude by ≥3 MAD; that is, a robust z-score of ≥3 or ≤-3. Network analysis was performed using STRING 9.1 (32). For kinase inhibitor dose responses, at least two independent measurements, each with duplicates were performed to calculate the mean responses and associated standard deviations.

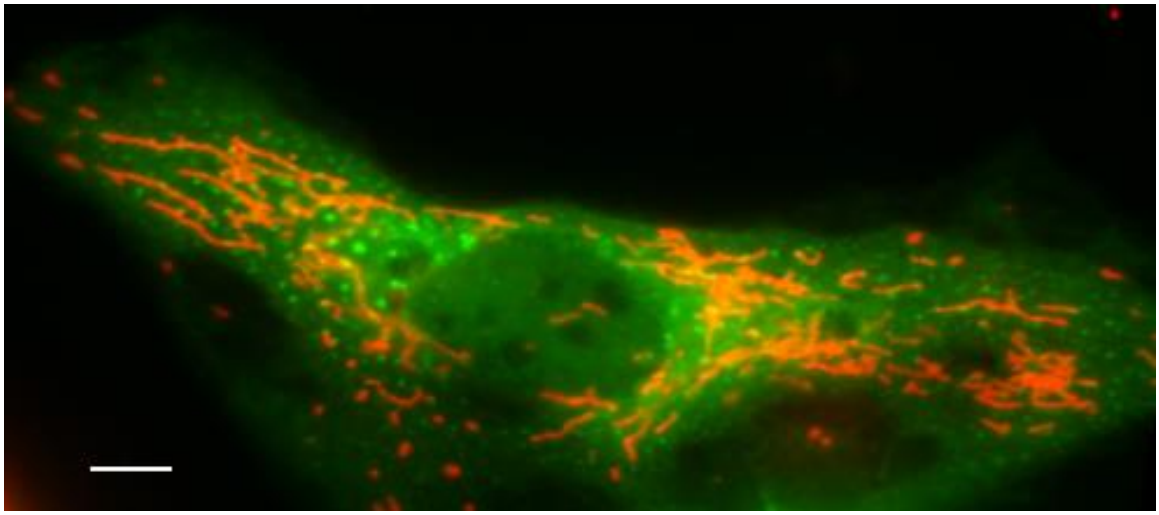

Fig. S1.

Conventional fluorescence microscope image of purinosomes (FGAMS-GFP, green) and mitochondria (MitoTracker Red, red) colocalization in HeLa cells grown under purine-depleted conditions. Scale bar: 3 μm.

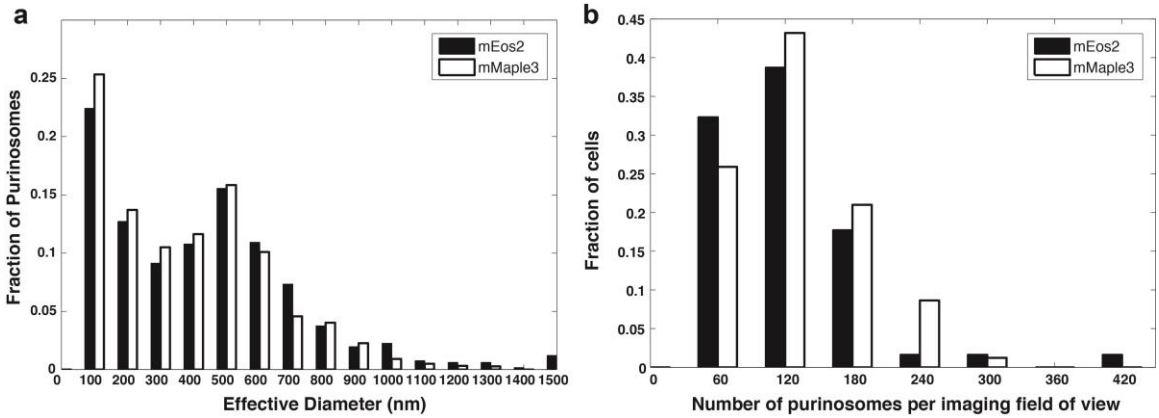

Fig. S2.

Distribution of purinosome size and number measured using different photoactivatable fluorescent proteins fused to FGAMS. Images of purinosomes collected using FGAMS-mEos2 fusion (black bars, $N = 22$) were compared to images collected using FGAMS-mMaple3 fusion (white bars, $N = 24$) in a Lesch-Nyhan disease fibroblast model *(12)*. No appreciable difference in a purinosome's effective diameter (**A**) or the number of purinosomes per imaging field of view (**B**) was observed.

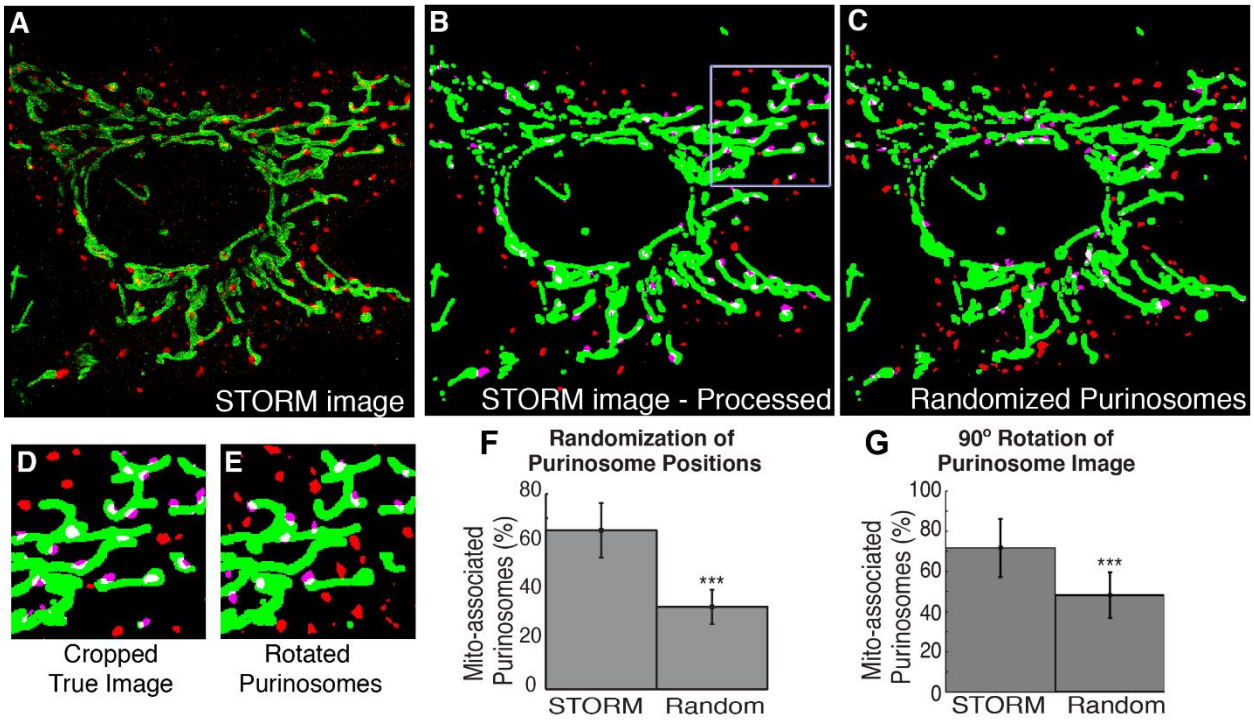

Fig. S3.

Analysis of purinosome and mitochondria colocalization. (**A**) The observed STORM image originally presented in Fig. 1A. (**B**) Colocalization analysis of the STORM image in Fig. 1A as described in the *Materials and Methods*. The purinosomes scored as colocalized are displayed in magenta. To determine colocalization significance, we used two methods to simulate a random distribution of purinosomes. First, we randomized the centroid positions of the imaged purinosomes within the cell boundary. An example image of a simulated random purinosome distribution shown in (**C**). Again, purinosomes scored as colocalized are displayed in magenta. The second method of randomization used was to identify the largest contiguous square region within the cell boundary [boxed region in (B), zoom in (**D**)] and rotate the purinosome image 90 degrees with respect to the mitochondria distribution (**E**). (**F**) Colocalization percentage determined from the STORM images is compared with that determined after the purinosome positions were randomized using the first method. The data reflects the mean ± standard deviation for all images (N = 26 images, also displayed in Fig. 1E, paired t-test, $p<0.001$ as denoted by ***) (**G**) As in (F) but the purinosome positions were randomized using the second (90-degree rotation) method (N=26 images, paired t-test, $p<0.001$ as denoted by ***). The colocalization percentages between the two randomization methods vary because the rotation method requires sub-sampling the image to a smaller square cropped region. This requirement biases the analysis towards the perinuclear region of the cell where the mitochondria density is often higher. However, both randomization methods clearly showed that the fraction of purinosomes colocalized with mitochondria in the STORM images is statistically significantly larger than that observed in the images where the purinosomes were randomized.

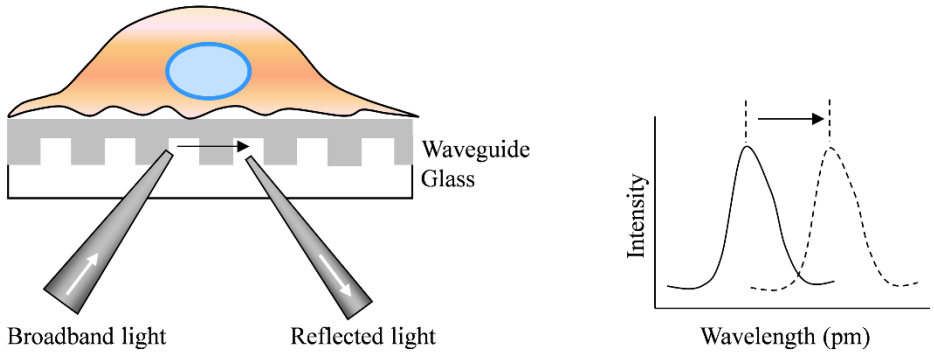

Fig. S4.

Principle of dynamic mass redistribution assay. DMR assay employs a resonant waveguide (RWG) biosensor to monitor, in real-time, any change in the local index of refraction within the bottom portion of living cells (~200 nm from the sensor surface). The RWG biosensor uses its diffractive nanograting to couple light into its waveguide thin film, generating a surface bound evanescent wave that is sensitive to local index of refraction. The coupled resonant light is propagated within the waveguide, eventually leaks out and is reflected back. The wavelength of the reflected light is tracked. The living cells are directly cultured and adherent onto the waveguide surface. Given that the index of refraction within a given volume of a cell is directly proportional to the concentration of biomacromolecules or mass density, the biosensor records compound-induced dynamic mass redistribution (DMR) signal as a dynamic shift in resonant wavelength (in picometers).

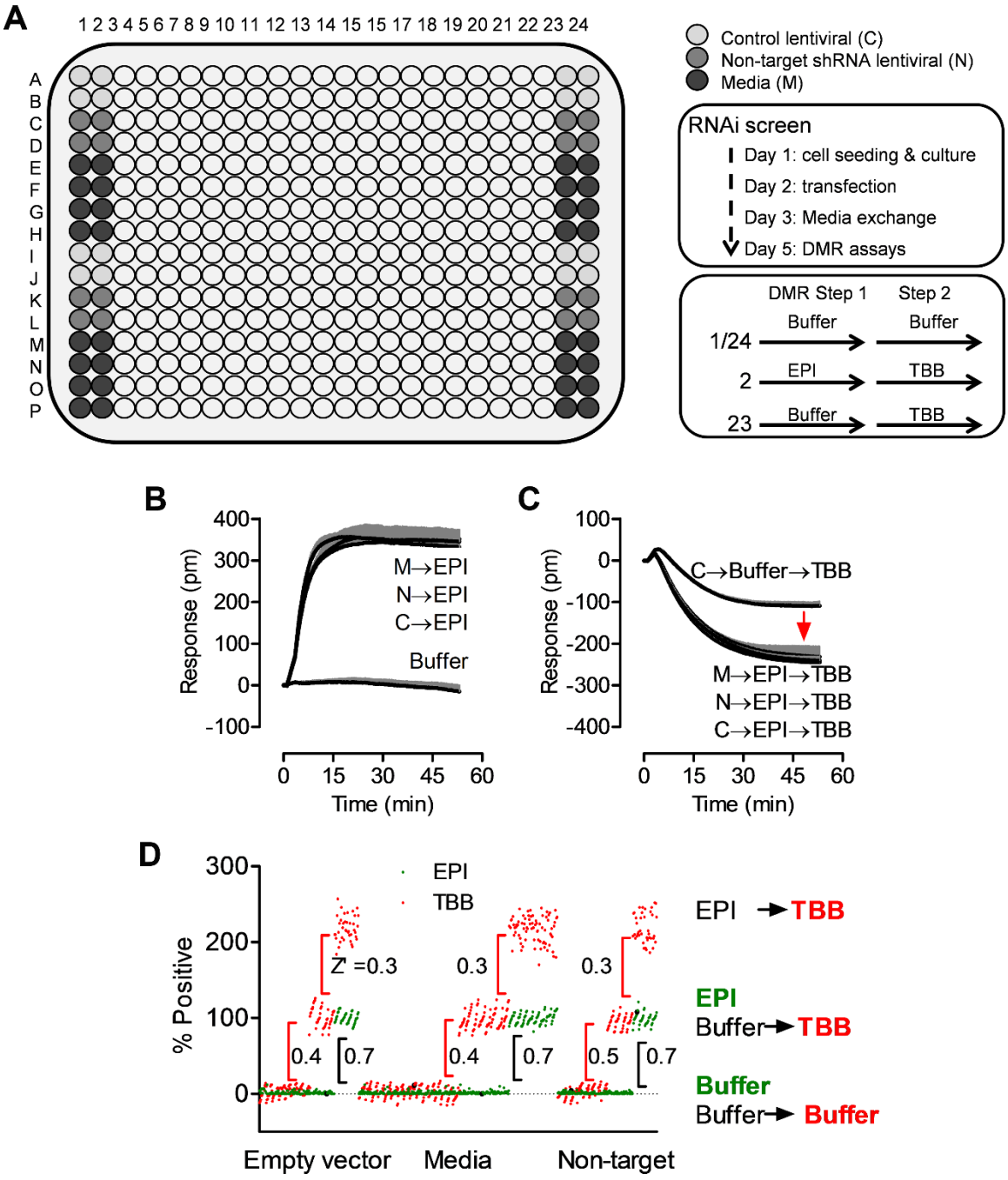

Fig. S5.

shRNA screening using two-step DMR assays.(**A**) Typical plate layout wherein within the plate there were 340 shRNA clones, each in singlet. Columns 1 and 24 were negative controls, wherein each well was sequentially treated with the assay buffer only. Column 2 was positive controls, wherein each well was sequentially treated with 100 nM EPI, and 20 μM TBB. Column 23 was controls for TBB, wherein each well was sequentially treated with the assay buffer and 20 μM TBB. We included three types of shRNA controls; that is, wells treated with the control lentivirus (C), non-target shRNA lentivirus (N), or media (M). All wells were pretreated with shRNA at day 2, followed by 3 days

transfection and culture. (**B**) The real-time DMR induced by 100 nM EPI or buffer, wherein EPI triggered almost identical DMR in the M, N, or C-treated cells, but the buffer triggered little DMR. (**C**) The real-time DMR induced by 20 μM TBB after pretreated with 100 nM EPI or buffer, wherein TBB triggered a negative DMR in the buffer pretreated cells, but a greater negative DMR in the EPI pretreated DMR. (**D**) The assay robustness as determined by Z' factor through comparison the DMR of EPI or TBB in the M, N, or C treated cells. For better illustration, all signals are normalized to the corresponding median DMR response obtained in the media treated cells to obtain the percentage of the positive response (% positive). For step 1, the median DMR of EPI in the media treated cells was set to 100% while for step 2, the median DMR of TBB after buffer pretreatment in the media treated cells was set to 100%. Since only the EPI DMR showed robustness in the entire screening assay (Z' factor > 0.5), an intra-plate normalization approach (described in methods) was required to identify hits.

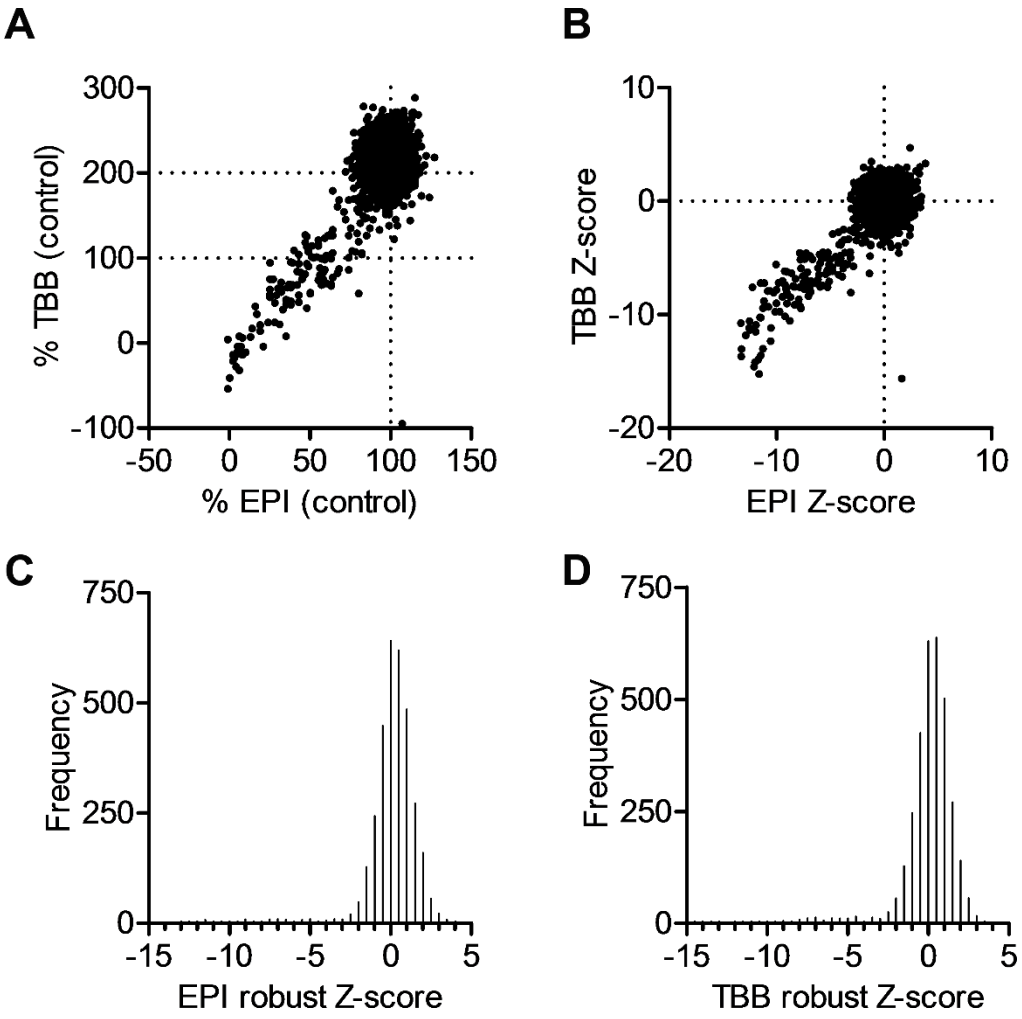

Fig. S6.

Impact of human kinome shRNA on the EPI- and TBB-induced DMR. (**A**) The correlation between percentages of the EPI DMR in the shRNA-treated cells and the TBB DMR in the shRNA-treated and EPI pre-stimulated cells. Here, we used an intra-plate referencing to normalize each response. Specifically, the DMR of EPI in the shRNA treated cells was normalized to the corresponding response in the non-target shRNA treated cells within the same plate (100%), while the DMR of TBB after EPI pre-stimulation in the shRNA-treated cells was normalized to the response of TBB after buffer pretreatment in the non-target shRNA treated cells (100%). A percentage of less than 100% for EPI indicates inhibition of the EPI-induced DMR by shRNA. Given that the EPI pretreatment increased the TBB DMR over 2-fold (Fig. S5C), a percentage of less than 200% of the control EPI-potentiated TBB DMR for TBB indicates inhibition of the EPI-potentiated TBB DMR by shRNA. (**B**) The correlation between the robust z scores of EPI and TBB, wherein the effect of shRNA on the EPI- and TBB-induced DMR were assayed, normalized by plate, and converted to robust z-scores. (**C**) The distribution of robust z-score for the EPI DMR. (**D**) The distribution of robust z-score for the TBB DMR after EPI stimulation. For (C) and (D), these robust z-scores were grouped into bins of 0.5 units and plotted as a histogram to show the range of robust z-scores.

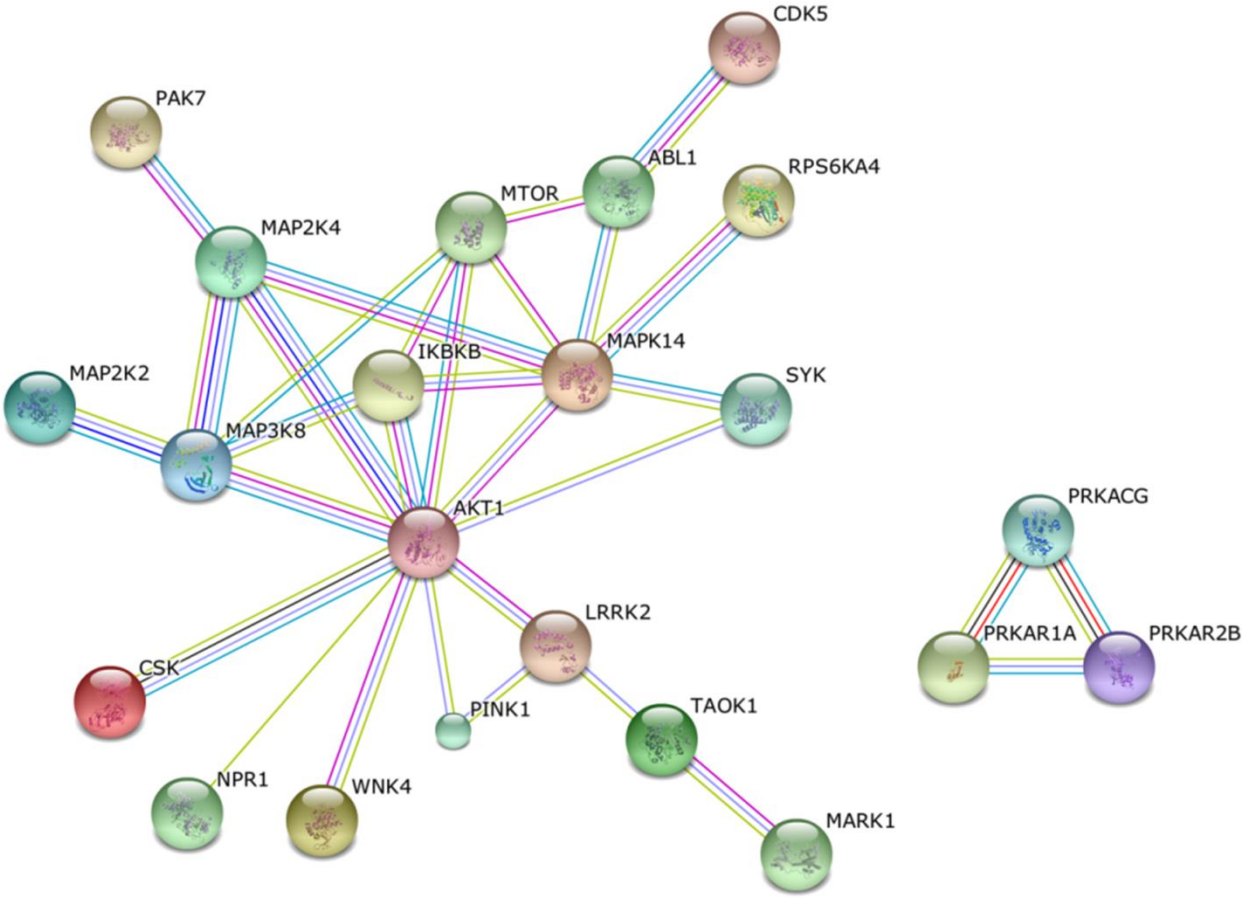

Fig. S7.

Kinase network of hits for the epinephrine-induced DMR. All hits identified were to inhibit the EPI-induced DMR. The network was generated using STRING 9.1. Connecting lines are color coded by the type of evidence used to build the network (details can be found in http://string-db.org/).

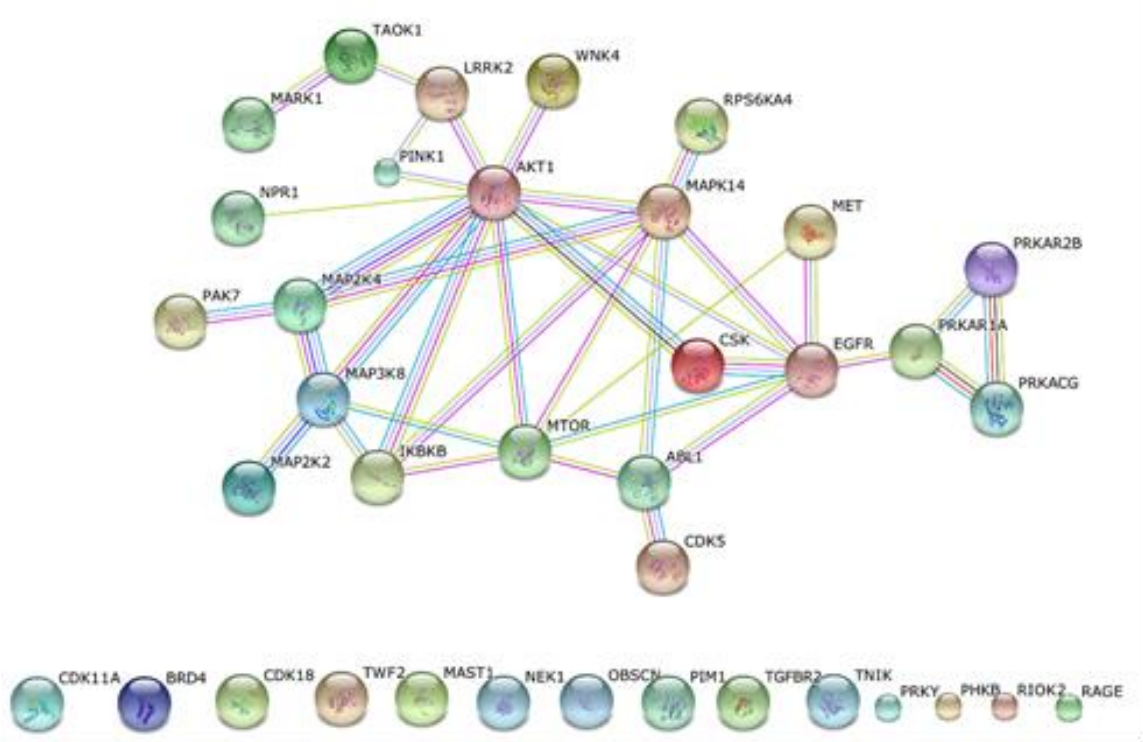

Fig. S8.

Kinase network of hits for the TBB-induced DMR after EPI pre-stimulation. All hits identified were to inhibit the TBB-induced DMR. The network was generated using STRING 9.1. Connecting lines are color coded by the type of evidence used to build the network (details can be found in http://string-db.org/). Unconnected hits were listed in the bottom row.

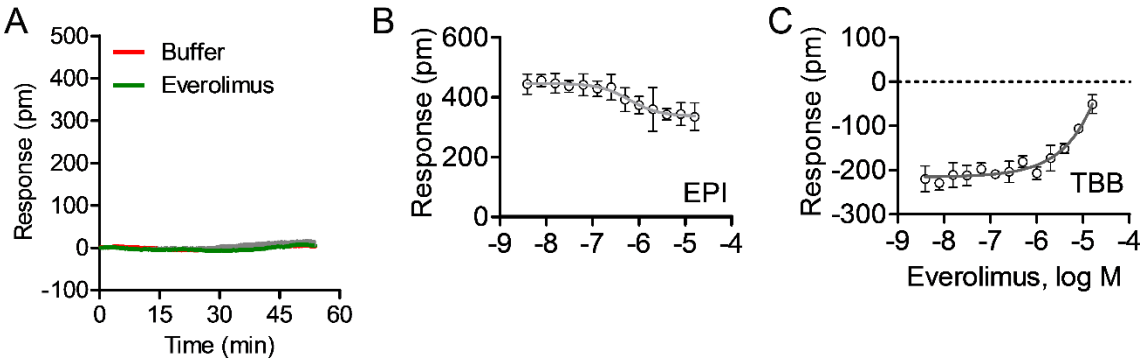

Fig. S9.

The impact of mTOR inhibitor everolimus on the EPI- and TBB-induced DMR. (**A**) The real-time DMR induced by everolimus or the assay buffer. (**B**) The dose effect of everolimus on the EPI DMR. (**C**) The dose effect of everolimus on the TBB DMR after EPI pre-stimulation. For both EPI and TBB their DMR amplitudes at 50min post stimulation were used for analysis. Results showed that everolimus alone did not trigger a DMR, but partially inhibited the EPI DMR and suppressed the EPI-potentiated DMR of TBB in a dose-dependent manner. Data represent mean ± SD. N = 4 (2 independent measurements, each in duplicate).

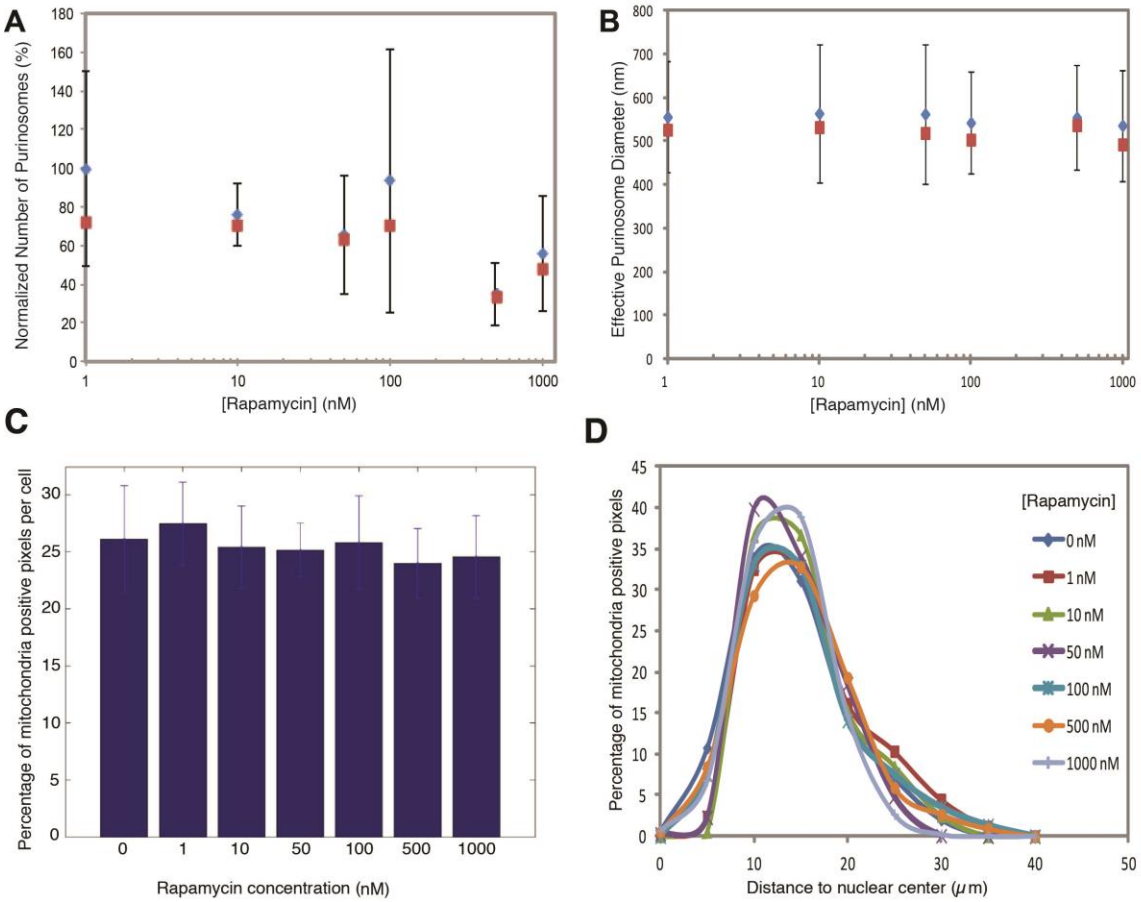

Fig. S10.

Rapamycin treatment does not substantially alter purinosome content or size and mitochondria content or distribution observed in STORM images. (**A**) Normalized purinosome number per field of view as a function of rapamycin concentration. The mean (blue diamonds) and median (red squares) numbers of purinosomes per field of view are both normalized to the mean number of purinosomes at 0 nM rapamycin. Error bars are standard deviations (N = 5 images per condition). (**B**) The average effective purinosome diameter in cells as a function of rapamycin concentration. Mean ± standard deviation (blue diamonds) and median (red squares), N=5 images per condition. (**C**) The fraction of mitochondria positive pixels per cell, calculated from STORM images, does not change appreciably over the range of rapamycin concentrations tested. Percentage reflects the mean ± standard deviation for all images (N=5 images per condition). (**D**) The radial distribution of mitochondria, calculated from the nuclear center, is not grossly altered by rapamycin treatment over the range of concentrations tested. Variations in the distribution can be attributed to a diversity of cell morphologies but in all cases the mitochondria distribution peaks at approximately 10-15 microns from the nuclear center and gradually decreases.

Table S2.

The gene names, shRNA clones, and robust z-scores for the kinase hits identified for the EPI- and TBB-induced DMR. These hits were identified when at least two shRNA clones for a single kinase within the library altered the EPI- or TBB-induced DMR by ≥3 MAD (median absolute deviation); that is, a robust z-score of ≥3 or ≤-3. Results showed that most kinases identified are common to both DMR, and only two kinases (NEK6 and SYK, green) are specific to the EPI-induced DMR, but four kinases (EGFR, MET, OBSCN and RAGE, red) are specific to the TBB DMR after EPI pre-stimulation.

Gene	Clone	EPI Z' score	TBB Z' score
ABL1	NM_005157.2-1226s1c1, NM_005157.2-3620s1c1 NM_005157.2-716s1c1, NM_005157.2-950s1c1	-1.3, -3.2 -7.6, -7.8	-3.8, -2.6 -6.6, -7.6
AKT1	NM_005163.x-954s1c1, NM_005163.x-1044s1c1	-7.4, -10.6	-7.8, -12.3
BRD4	NM_058243.1-1485s1c1, NM_058243.1-4269s1c1	-5.8, -6.2	-4.8, -6.9
CDC2L2	NM_024011.1-2026s1c1, NM_024011.1-155s1c1	-8.5, -10.5	-7.5, -11.2
CDK5	NM_004935.2-954s1c1, NM_004935.2-481s1c1, NM_004935.2-837s1c1	-5.2, -7.2, -9.0	-4.5, -5.0, -9.0
CSK	NM_004383.x-633s1c1, NM_004383.x-876s1c1 NM_004383.x-903s1c1, NM_004383.x-1057s1c1	-5.4,-7.7 -11.5, -12.1	-6.4, -9.5 -13.6, -14.6
EGFR*	NM_005228.3-1246s1c1, NM_005228.3-1216s1c1	-1.8, -10.0	-3.5, -9.0
IKBKB	NM_001556.1-2278s1c1, NM_001556.1-1538s1c1	-3.2, -8.7	-4.5, -8.5
LRRK2	XM_058513.8-2128s1c1, XM_058513.8-6782s1c1	-11.2, -13.4	-8.8, -10.8
MAP2K2	NM_030662.2-1219s1c1, NM_030662.2-1221s1c1, NM_030662.2-1218s1c1	-8.4, -6.9, -9.8	-7.6, -8.0, -9.7
MAP2K4	NM_003010.2-991s1c1, NM_003010.2-1247s1c1	-4.6, -9.3	-4.9, -6.2
MAP3K8	NM_005204.x-1510s1c1, NM_005204.x-1602s1c1, NM_005204.x-1184s1c1	-9.2, -8.8, -11.7	-10.2, -10.6, -14.0
MAPK14	NM_139012.x-795s1c1, NM_139012.x-877s1c1	-7.3, -12.1	-6.9, -14.2
MARK1	NM_018650.2-1825s1c1, NM_018650.2-2586s1c1, NM_018650.2-1564s1c1	-5.3, -12.6, -13.3	-7.6, -11.2, -13.7
MAST1	NM_014975.1-1294s1c1, NM_014975.1-761s1c1, NM_014975.1-3235s1c1	-5.7, -5.7, -12.0	-4.5, -7.5, -11.5

MET	NM_000245.1-2037s1c1, NM_000245.2-4387s1c1	1.6, -12.3	-15.6, -7.6
MTOR	NM_004958.2-8344s1c1, NM_004958.2-2473s1c1, NM_004958.2-3425s1c1	-4.2, -4.0, -5.8	-3.8, -3.9, -5.0
NEK1	NM_012224.1-4290s1c1, NM_012224.1-1427s1c1, NM_012224.1-2206s1c1	-4.1, -5.7, -4.8	-4.8, -5.0, -5.8
NEK6	NM_014397.x-445s1c1, NM_014397.x-1888s1c1	3.8, 3.3	3.3, 2.4
NPR1	NM_000906.2-3198s1c1, NM_000906.2-1418s1c1	-7.6, -6.0	-7.2, -7.6
OBSCN	NM_052843.1-15939s1c1, NM_052843.1-6870s1c1	-2.6, -5.2	-3.5, -6.1
PAK7	NM_020341.2-2163s1c1, NM_020341.2-616s1c1	-12.5, -12.5	-10.6, -11.3
PCTK3	NM_002596.1-718s1c1, NM_002596.1-2507s1c1	-7.2, -6.3	-6.3, -7.2
PHKB	NM_000293.1-3514s1c1, NM_000293.1-3101s1c1, NM_000293.1-3455s1c1	-3.7, -6.7, -6.1	-4.5, -5.1, -6.5
PIM1	NM_002648.x-644s1c1, NM_002648.x-553s1c1	-7.1, -8.4	-8.4, -9.1
PINK1	NM_032409.1-284s1c1, NM_032409.1-608s1c1, NM_032409.1-1036s1c1	-4.0, -7.4, -13.3	-3.6, -5.1, -13.0
PRKACG	NM_002732.2-264s1c1, NM_002732.2-265s1c1	-6.9, -11.6	-4.8, -10.2
PRKAR1A	NM_002734.3-879s1c1, NM_002734.3-2211s1c1	-4.8, -11.5	-6.2, -10.3
PRKAR2B	NM_002736.2-1401s1c1, NM_002736.2-518s1c1	-4.0, -7.9	-3.6, -4.6
PRKY	NM_002760.2-1030s1c1, NM_002760.2-1085s1c1	-3.4, -10.2	-5.6, -9.8
RAGE	NM_014226.x-450s1c1, NM_014226.x-1402s1c1	-0.4, -1.3	-3.9, -4.8
RIOK2	NM_018343.1-177s1c1, NM_018343.1-1604s1c1	-6.0, -7.5	-4.7, -6.6
RPS6KA4	NM_003942.2-2193s1c1, NM_003942.2-170s1c1, NM_003942.2-2003s1c1	-9.1, -11.2, -11.3	-6.2, -7.2, -9.4
SYK	NM_003177.3-2181s1c1, NM_003177.3-2506s1c1	-3.8, -9.5	-2.5, -8.4
TAOK1	NM_020791.1-1462s1c1, NM_020791.1-1671s1c1	-6.9, -8.2	-4.8, -6.9
TGFBR2	NM_003242.4-484s1c1, NM_003242.4-3061s1c1	-6.2, -9.3	-5.9, -7.3
TNIK	XM_039796.9-2358s1c1, XM_039796.9-3935s1c1, XM_039796.9-931s1c1	-5.1, -10.8, -11.9	-5.6, -9.3, -10.9
TWF2	NM_007284.3-897s1c1, NM_007284.3-610s1c1	-3.8, -5.9	-5.9, -7.5

WNK4	NM_032387.2-534s1c1, NM_032387.2-1590s1c1, NM_032387.2-723s1c1	-5.2, -9.8, -12.9	-6.0, -7.2, -11.8

Table S3.

Gene-ontology (GO) term analysis based on the kinase hits identified. The identified kinase hits were entered into a GO term enrichment analysis tool. GO terms (cellular processes) with a p-value close to zero show a greater significance of being associated with genes of the kinases identified. For the EPI response, NPR1, ABL1, MOTR and LRRK2 were implicated in regulation of purine nucleotide metabolic process; for the TBB response, beside these four kinases, OBSCN (cytoskeletal calmodulin and titin-interacting RhoGEF) was also implicated in regulation of purine nucleotide metabolic process, according to GO biological process enrichment analysis using String 9.1.

GO term	Biological process	p-value
EPI DMR		
GO:0006468	protein phosphorylation	7.44E-22
GO:0032270	positive regulation of cellular protein metabolic process	7.54E-13
GO:0006796	phosphate-containing compound metabolic process	8.24E-13
GO:0006793	phosphorus metabolic process	1.12E-12
GO:0051338	regulation of transferase activity	2.47E-12
GO:0051247	positive regulation of protein metabolic process	2.91E-12
GO:1900542	regulation of purine nucleotide metabolic process	8.91E-3
TBB DMR		
GO:0006468	protein phosphorylation	2.79E-21
GO:0045937	positive regulation of phosphate metabolic process	5.93E-16
GO:0051347	positive regulation of transferase activity	3.86E-14
GO:0032270	positive regulation of cellular protein metabolic process	2.02E-12
GO:0006796	phosphate-containing compound metabolic process	3.09E-12
GO:0006793	phosphorus metabolic process	4.18E-12
GO:0051338	regulation of transferase activity	6.11E-12
GO:0051247	positive regulation of protein metabolic process	7.76E-12
GO:1900542	regulation of purine nucleotide metabolic process	1.66E-3

Additional Data Table S1 (separate file)

Proteins identified from isolated mitochondria under conditions favoring purinosome formation. The name, accession number, and molecular weights of the identified proteins are given followed by four pairs of data corresponding to the mitochondrial fraction (-in-gel) and cytoplasmic fraction (-in-solution) for each of the four chemical cross-linking experiments conducted. The values are percent sequence coverage for the listed proteins.